Applied Surface Science 258 (2012) 6730–6734

Contents lists available at SciVerse ScienceDirect

Applied Surface Science

journal homepage: www.elsevier.com/locate/apsusc

Nanoindentation response of zinc titanate thin films deposited by co-sputtering process

Shyh-Chi Wu [a,b], Yeau-Ren Jeng [c], Wei-Hung Yau [d], Kuan-Te Wu [c], Chien-Huang Tsai [e,*], Chang-Pin Chou [a]

[a] Department of Mechanical Engineering, National Chiao Tung University, Hsinchu 300, Taiwan, ROC
[b] Chung Shan Institute of Science and Technology (CSIST), Taoyuan 325, Taiwan, ROC
[c] Department of Mechanical Engineering, National Chung Cheng University, Chia-Yi 621, Taiwan
[d] Department of Mechanical Engineering, Chin-Yi University of Technology, Taichung 400, Taiwan, ROC
[e] Department of Automation Engineering, Nan Kai University of Technology, Nantou 54243, Taiwan, ROC

ARTICLE INFO

Article history:
Received 4 October 2011
Received in revised form 16 February 2012
Accepted 16 February 2012
Available online 21 March 2012

Keywords:
Radio frequency magnetron co-sputtering
Hardness
Atomic force microscopy
X-ray photoelectron spectroscopy

ABSTRACT

In this study, $ZnTiO_3$ films were grown by radio frequency magnetron co-sputtering using a sintered ceramic target on silicon substrates, we used nanoindenter techniques under a CSM mode to evaluate the hardness (H) and elastic modulus (E) of the films after annealing in temperature range of 520–820 °C. The measured values of hardness and elastic moduli of the $ZnTiO_3$ films were in the range from 8.5 ± 0.4 to 5.6 ± 0.4 GPa and from 171 ± 2.3 to 155 ± 2.5 GPa, respectively. It is evident that an increase in the roughness due to high annealing temperature using atomic force microscopy. The XRD patterns were observed that as-deposited films are mainly amorphous, however, the hexagonal $ZnTiO_3$ phase was observed with the $ZnTiO_3$ (1 0 4), (1 1 0), (1 1 6), and (2 1 4) peaks from 620 to 820 °C, indicating that there is highly (1 0 4)-oriented $ZnTiO_3$ on the silicon substrate. The X-ray photoelectron spectroscopy core level analysis of the $ZnTiO_3$ films have been measured for O 1s that can be attributed the weaker bonds and lower resistance at the film based on the higher annealed temperature. The H, M, R_{ms}, and R_a were altered due to the grain growth and recovery to result in a relax crystallinity at $ZnTiO_3$ films.

© 2012 Elsevier B.V. All rights reserved.

1. Introduction

$ZnO–TiO_2$ system is attractive because of their outstanding performance as an inorganic compound. Above of them, $ZnTiO_3$ film was found to be zinc metatitanate with a hexagonal structure and titanium dioxide while the film of Zn/Ti ratio is lower than 1. The zinc titanate phases found in the films depend primarily on the film stoichiometry. The introduction of three compounds existing in the $ZnO–TiO_2$ system has been reported in previous study [1], such as-Zn_2TiO_4 (cubic), $ZnTiO_3$ (hexagonal), and $Zn_2Ti_3O_8$ (cubic). Fundamental studies is concerned because of its diverse electrical and chemical properties, leading to the commercial applications, such as white pigment, catalytic sorbent [2–4], microwave dielectric materials [5–7], gas sensor [8], and high performance catalysts [9–11]. Beside, the luminescent application could be induced by the $ZnTiO_3$ doped with some transition metal ions [12,13]. $ZnTiO_3$, preparation by solid state reaction, was reported by means of sol–gel [12,14,15], bulk manufacture [16,7,17], and chemical vapor deposition [18]. However their studies are limited to the analyses of phase, composition, and microstructure of the film. There are few reports concerning the nanohardness of $ZnTiO_3$ system in literatures, except these properties–structures, grain sizes, and morphologies that can be enhanced through their extrinsic properties.

In this study, the authors have attempted to synthesize $ZnTiO_3$ film by RF magnetron co-sputtering process. We employed nanoindentation techniques to discover the response of $ZnTiO_3$ film; their surface roughness, crystallization, and chemical bonding were analyzed by using atomic force microscopy diffraction, X-ray diffraction, and X-ray photoelectron spectroscopy. The qualities of the resulting $ZnTiO_3$ films, in terms of phase present under annealing treatment, were examined.

2. Experimental details

The $ZnTiO_3$ films were prepared by RF magnetron co-sputtering system using 4-inch-diameter sintered ceramic target (Zn and Ti). In order to obtain stoichiometric deposit $ZnTiO_3$ films on Si substrate, $Ar–O_2$ flow (8:2) with a purity of 99.999 gas of 50 sccm was introduced into the chamber with mass flow controllers and, RF powers at 200 W were used. In addition, the sputtering pressure was 2×10^{-2}, the substrate temperature was set at 250 °C, and

* Corresponding author.
E-mail address: chtsai12@gmail.com (C.-H. Tsai).

0169-4332/$ – see front matter © 2012 Elsevier B.V. All rights reserved.
doi:10.1016/j.apsusc.2012.02.076

Table 1
RF sputter conditions for the zinc titanate films.

Target	$ZnTiO_3$
Target size in diameter (in.)	4
Target to substrate distance (mm)	90
RF power (W)	200
Chamber pressure (Torr)	5×10^{-6}
Working pressure (Torr)	2×10^{-6}
Sputtering gas	Ar
$Ar–O_2$ flow (seem)	50 (8:2)
Substrate temperature (°C)	250
Deposition time (min)	120

the duration of the deposition was 1 h. To remove the contaminants formed on the target surface and to stabilize the sputtering conditions, it was necessary for pre-sputtering to be performed for 5 min prior to each deposition process. Those specimens were subsequently subjected to *ex situ* thermal treatment in a furnace under N_2 gas for 2 h with a heating rate of 5 °C/min at 520, 620, 720, and 820 °C, respectively. The detailed deposition conditions of the $ZnTiO_3$ films are listed in Table 1.

After deposition, the surface roughness and microstructure are analyzed using AFM (Veeco Dimension 5000, Scanning Probe Microscopy, D5000). The values of *H* and *M* of the $ZnTiO_3$ films were determined using a Nano Indenter XP instrument (MTS Cooperation, Nano Instruments Innovation Center, TN, USA). The nanoindentation was performed using a diamond Berkovich indenter tip (tip radius: ca. 50 nm); plastic deformation was generated at very small loads. The continuous contact stiffness measurement (CSM) mode, which is executed by superimposing small oscillations on the force signal to measure displacement responses, offers a direct measurement of dynamic contact stiffness during the loading process in the indentation test [19]. Chemical bonding states and chemical compositions of the films were analyzed by X-ray photoelectron spectroscopy (XPS, VG Scientific Microlab 310F). Inductively coupled plasma-mass ICP spectrometer was applied to determine the elements concentrations in the films, which confirmed the stoichiometry of $ZnTiO_3$. Crystallinity of the films were analyzed by X-ray diffraction (PANalytical X'Pert Pro (MRD), with Cu Kα (λ = 0.154 nm) radiation for 2θ from 20° to 80° at a scan speed of $2° \min^{-1}$, and a grazing angle of 0.5° under 30 kV and 30 mA.

3. Results and discussion

Fig. 1 shows AFM inspections of $ZnTiO_3$ films deposited with silicon substrate. The surface roughness of $ZnTiO_3$ films is increased from 3, 3, 3.9, and 5.8 to 20.6 nm as the annealing temperature increased from RT to 820 °C. Clearly, as the annealing temperature was increased, surface morphologies of the samples became rough and grains grew. The corresponding AFM observations demonstrate that there are many small cavities and bright particles in the film after annealing treatment, particular start at 620 °C. From previous articles [20–22], the similar phenomenon was observed that the cavities are due to the evaporation of Zn, and the white particles are TiO_2. Furthermore, it appears that a high annealing temperature

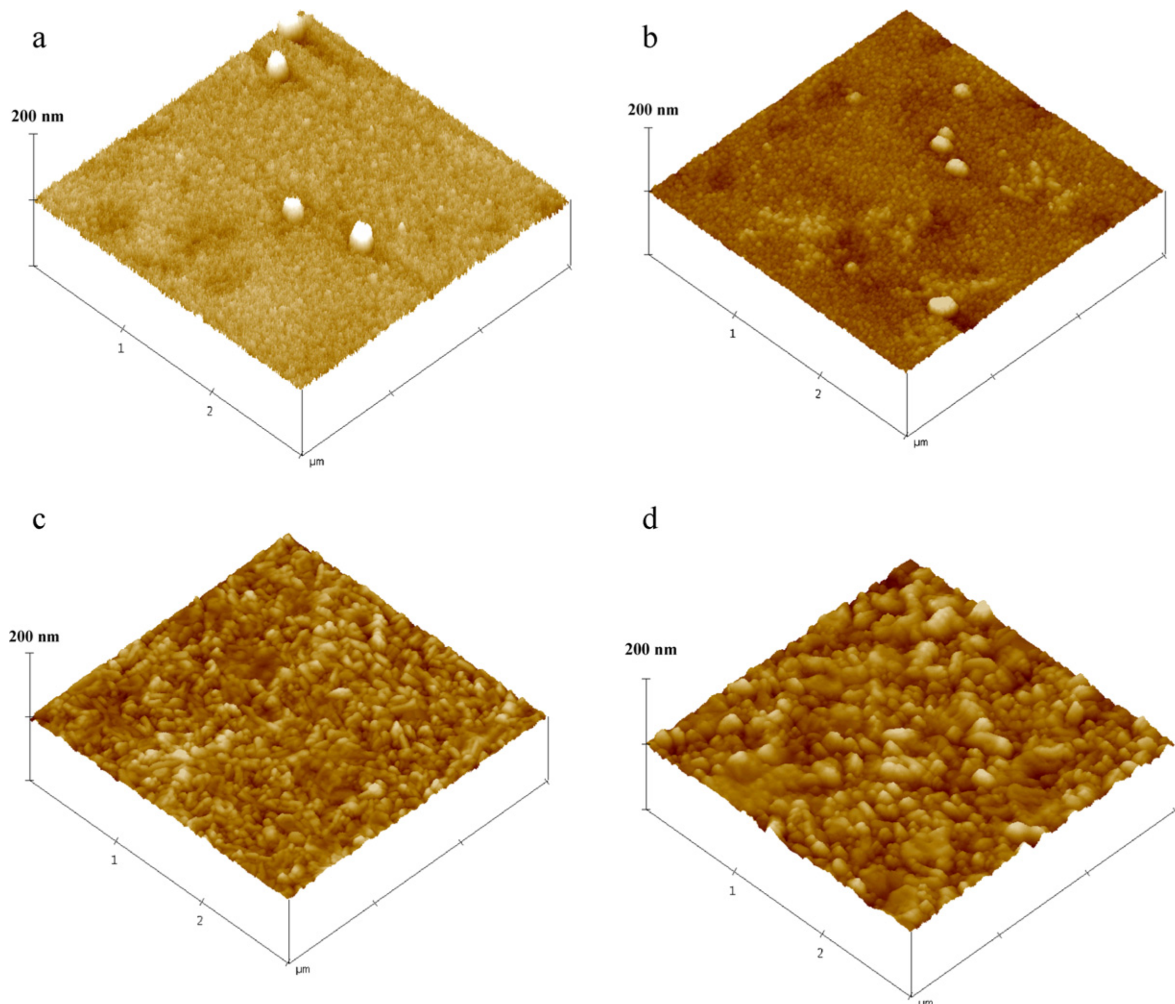

Fig. 1. 3D-AFM images of the surfaces of $ZnTiO_3$ films: (a) RT, (b) 520, (d) 620, (e) 720, and (f) 820 °C.

favors a particle with larger grain sizes at 820 °C and more densely than that of low annealing temperatures. The experiments clearly demonstrated that the crystalline structure and surface roughness of $ZnTiO_3$ film can be clearly changed. It suggests that a high annealing temperature enhanced the atomic mobility and caused the grain recovery to result in a relax crystallinity. The subsequent results of XRD will be discussed as well.

To study the nanomechanical properties of the $ZnTiO_3$ film, nanoindentation was employed to measure the values of H and E upon varying conditions. Fig. 2(a) and (b) display the variation in nanohardness H (GPa) and Young's modulus E (GPa) with respect to the $ZnTiO_3$ film. It is determined that the values of H and E of the $ZnTiO_3$ film with respect to the indentation depth, following the method proposed by Oliver and Pharr [20]. For indentation depths up to 5 nm, the values of H increased upon increasing the indentation depth; this can be attributed to the transition between purely elastic and elastoplastic contact, whereas the value of H is actually equal to the contact pressure [16]. While the indentation depths over 50 nm, the H tends to constant. We respect that a strengthening effect is dominated from the strain or strain rate hardening. The H and E were calculated by averaging measurements at indentation depths ranging from 80 to 180 nm. The depths of the film thickness not exceeding 20% that can be attributed to access a fully plastic zone and to avoid the substrate effect [19]. For thermal treatment at RT, 520, 620, 720, and 820 °C, the values of H of the $ZnTiO_3$ film were 8.5 ± 0.4, 11.4 ± 0.4, 10.5 ± 0.4, 9.6 ± 0.5, and 5.6 ± 0.4 GPa, respectively, while those of E were 171 ± 2.3, 178 ± 2.4, 202 ± 3.5, 198 ± 3.2, and 155 ± 2.5 GPa, respectively. Markedly, in metal oxides the intrinsic defects such as oxygen vacancies and metal ion interstitials usually coexist. We conclude that the lower values of H and E of the $ZnTiO_3$ film can be induced by some reason, including the packing factor, stoichiometry, residual stress, preferred orientation, and grain size [23]. A low value of R_{ms} is beneficial to a $ZnTiO_3$ film because it can be used to provide information regarding its morphology; the surfaces morphologies of our films were relatively rough and non-uniformly distributed. In addition, the grain size in the $ZnTiO_3$ film increases obviously when annealing temperature is higher, casing many gaps between grain boundaries due to the abnormal grain growth. We indicate that the structure of $ZnTiO_3$ films changes with annealing atmosphere, which induces the variation of the concentration of intrinsic defects. Fig. 2(c) presents the load/displacement P–h curve recorded during the indentation process; it reached a maximum indentation load of 9 mN. We obtained discordant curves and irregularities appeared in the course of plastic deformation, which is characterized by the continuities at penetration depths, for the typical loading/unloading process. It is suggested that the curve implies a trend of gradual elastic deformation. We also observed a larger deviation in the P–h curves of the $ZnTiO_3$ films that had been subjected to various loading/unloading. Nanoindentation result reveals a variation of compressive stress transition around the indentation regions of the $ZnTiO_3$ films. The initial deformation, elastic deformation, and residual deformation of the $ZnTiO_3$ films were evaluated based on the thermal treatment. The elastic modulus is a fundamental property that is influenced by bonding between atoms. The stiffness or elastic modulus of a film depends upon the interatomic distances [23–25].

The constituent elements of the $ZnTiO_3$ films were measured. The chemical compositions of the films deposited at various annealing temperature were shown in Fig. 3. Jung et al. [28] conducted that a main phase $ZnTiO_3$ into Zn_2TiO_4 and TiO_2 occurred in association with the increase of annealing temperature. From earlier reports [27,28], the ceramic powder reaction can be displayed that the $ZnTiO_3$ phase decomposed to from Zn_2TiO_4 and rutile TiO_2 above 945 °C with increasing the annealing temperature. The trend of the increase in oxygen content (65–70%) is similar in our results while

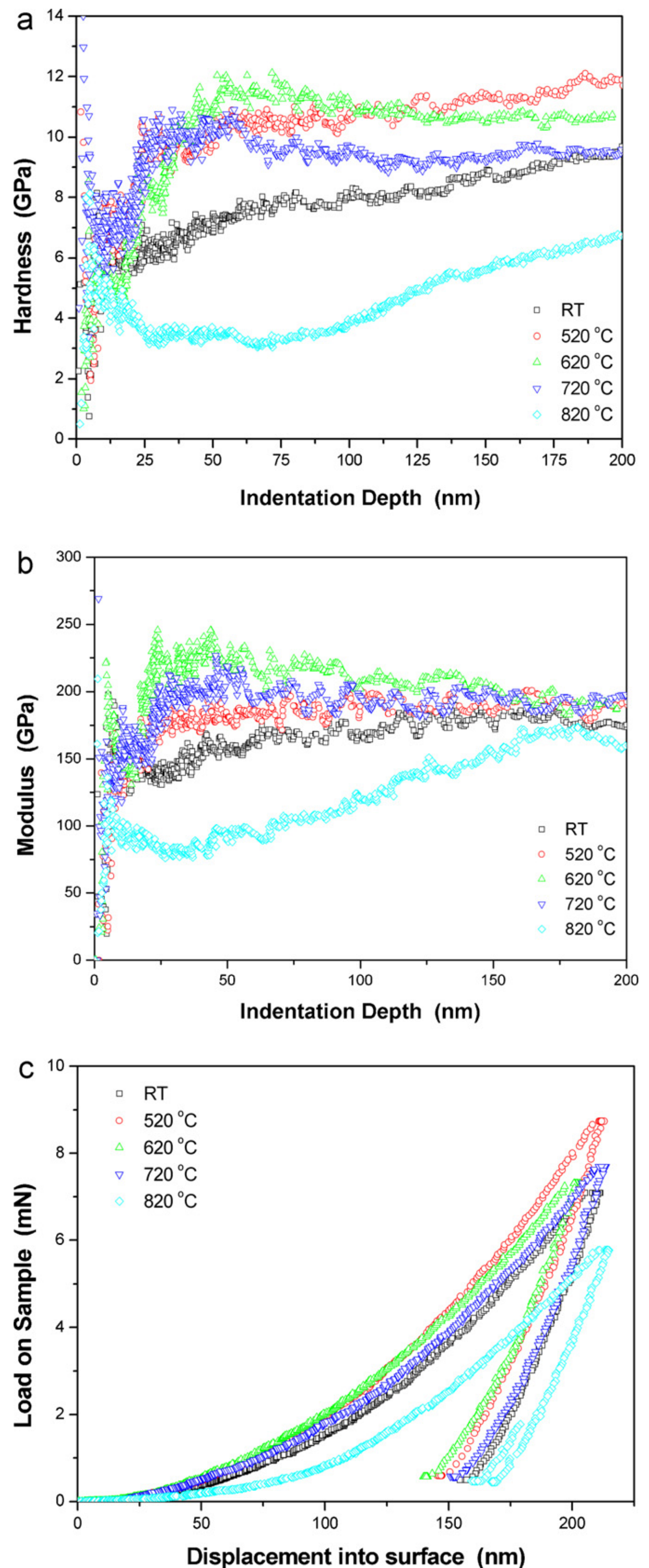

Fig. 2. (a) Hardness, (b) elastic moduli, and (c) displacements of loading–unloading curves of $ZnTiO_3$ films samples with respect to the variation of annealing condition: RT, 520, 620, 720, and 820 °C.

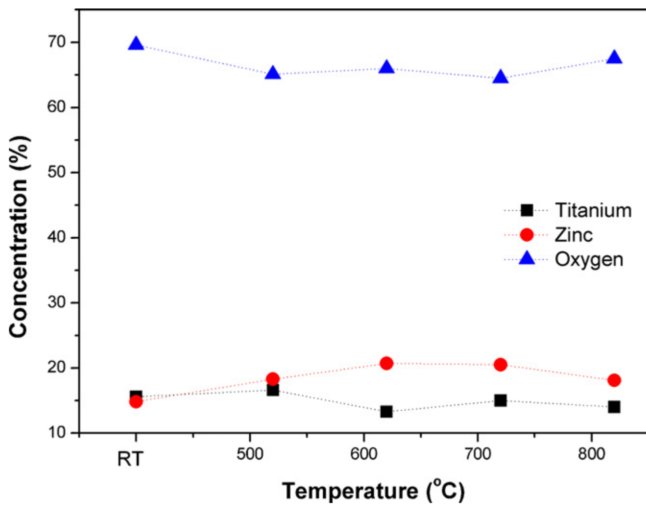

Fig. 3. The stoichiometric change of $ZnTiO_3$ thin films treated by conventional annealing condition: RT, 520, 620, 720, and 820 °C.

chemical compositions are changed based on annealing temperature. At the same time, chemical bonding states in the $ZnTiO_3$ films were characterized by XPS measurement, as shown in Fig. 4. The XPS spectra have been changed corrected to the adventitious O 1s. The binding energy of the O 1s state is located from 530 to 538 eV, which depended on the annealing temperature that splits in their peaks under various growth procedures of $ZnTiO_3$ films are clearly examined. One can observe a part of O—Zn bond formation (binding energy at 529.4 eV and 531.5 eV) at the annealing temperature from RT to 520 °C that the peak positions are in good agreement with the Zn—O bond and some Ti—O bond [1,29]. Apparently, the annealing temperature from 620 to 720 °C is evidence that the mains chemical bonding may be coexisting as Zn—O (binding energy at 531.5 eV) and Ti—O (binding energy at 533 and 536 eV). We can compare O 1s state at the 820 °C, the curve is significant shift into other zone due to more chemical impurity from Zn—O and Ti—O bond. In addition, O 1s state at the RT to 520 °C, the peak at 530.1 eV may be due to Zn—O bonds and significant peak at 531.8 eV is attributed as $MnCl_2$. The broad binding energy at 532–534 eV seen in O 1s spectrum is considered to be due to residual oxygen at the film surface, of which the binding energy is reported to be 532.8 eV [29,30]. Phani et al. [31] has discussed that stoichiometric change of $ZnTiO_3$ thin films could be treated by conventional annealing. The annealed

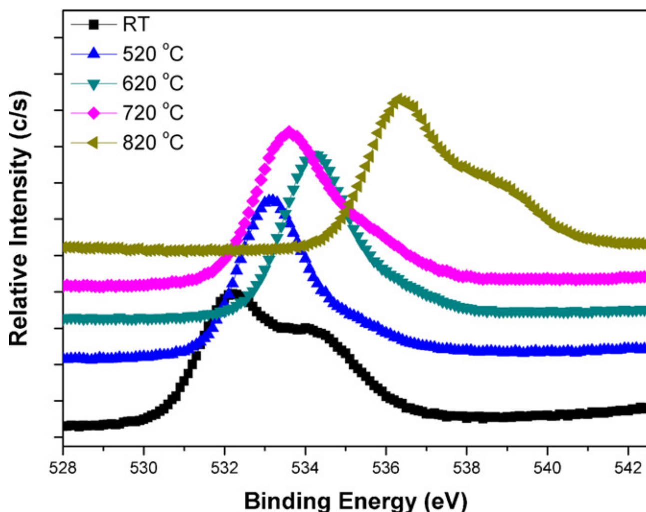

Fig. 4. XPS core level spectra (O 1s) of $ZnTiO_3$ films on Si substrate with respect to the variation of annealing condition: RT, 520, 620, 720, and 820 °C.

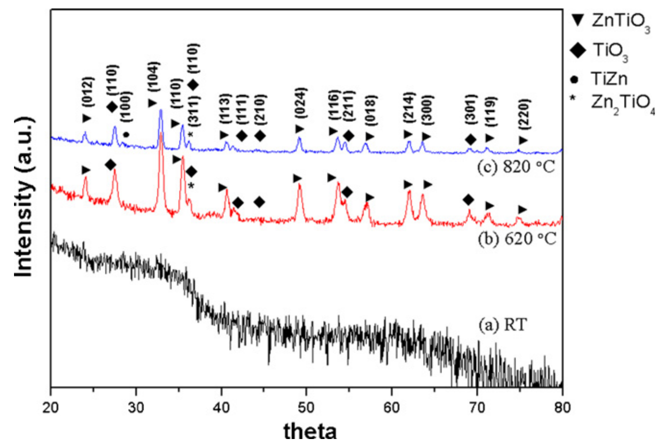

Fig. 5. X-ray diffraction patterns of the $ZnTiO_3$ films (a) as-deposited at RT, and different thermal temperatures (b) 620 and (c) 820 °C.

films have shown $ZnTiO_3$ cubic phase formation at and above 620 °C substrate temperature. The chemical 532.0 eV peak for $ZnTiO_3$ films are attributed to O—H bonds due to absorbed H—O molecules on the films. In addition, the peak appeared at 533.1 eV has been assigned to O 1s in SiO_2 that presented on the surface of the annealed films on Si substrate.

In Fig. 5, the XRD patterns of the $ZnTiO_3$ films: (a) as-deposited and the annealing treatment was (b) 620 °C and (c) 820 °C. It was observed that there were no diffraction peaks in the XRD pattern for as-deposited films (Fig. 3(a)). It is suggested that the film structure is mainly amorphous [16]. Herein, as the annealing treatment sample was 620 °C, the hexagonal $ZnTiO_3$ phase was observed with the $ZnTiO_3$ (1 0 4), (1 1 0), (1 1 6), and (2 1 4) peaks (Fig. 5(b)). The intensities of the (1 0 4) peak was higher than the other peaks of $ZnTiO_3$ films at 820 °C, indicating that there is highly (1 0 4)-oriented $ZnTiO_3$ on the silicon substrate. From recent reports [16], the preferred orientation tends to reduce its free energy to reach a stable state, this is the same case in our experimental data. The $ZnTiO_3$ structure is also comparable with the XPS that Zn-O and Ti-O binding energy at 533 and 536 eV is strongly as the annealing treatment sample was 620 °C. However, the low Zn—O and Ti—O binding energy is displayed due to more chemical impurity from XPS analysis; thus the ZnTi (1 1 0) structure has a weak diffraction peak in the XRD pattern at the 820 °C. We attributed that the hexagonal $ZnTiO_3$ decomposed into cubic Zn_2TiO_4 and TiO_2 (rutile), even the $ZnTiO_3$ phase remained stable at the temperatures of 820 °C [34].

Table 1 lists the summaries of H, M, R_{ms}, and R_a. $ZnTiO_3$ films often have different thermal properties, resulting in strain when the films are annealed under elevated temperatures. The crystal texture of $ZnTiO_3$ films can influence their mechanical properties at different annealing treatment stage; the comparison of phase transformation of $ZnTiO_3$ films was performed by XRD pattern as well. Grain growth and strain energy are processed at the inner film that can often be a dominant factor. Although we obtained appropriate information from XPS analysis, the deposition conditions affected not only depended on annealed temperature but also the Ti, Zn, and O compositions during the growth by RF magnetron

Table 2
The summaries of $ZnTiO_3$ film with respect to the H, M, R_{ms}, and R_a.

$ZnTiO_3$	Modulus (GPa)	Hardness (GPa)	R_{ms}	R_a
As-deposited	171 ± 2.3	8.5 ± 0.4	3	2.1
520 °C	178 ± 2.4	11.4 ± 0.4	3	2.2
620 °C	202 ± 3.5	10.5 ± 0.4	3.9	3.1
720 °C	198 ± 3.2	9.6 ± 0.5	5.8	4.6
820 °C	155 ± 2.5	5.6 ± 0.4	20.6	16.6

co-sputtering process. We attributed that oxygen chemisorbs with metal bond and cases a surface layer of adsorbed oxygen (Table 2).

4. Conclusion

We have characterized RF magnetron co-sputtering $ZnTiO_3$ films using AFM and nanoindenter techniques. The measured values of hardness and elastic moduli of the $ZnTiO_3$ films were in the range from 8.5 ± 0.4 to 5.6 ± 0.4 GPa and from 171 ± 2.3 to 155 ± 2.5 GPa, respectively. Slight oscillations and discontinuous phenomena in each hardness curve due to the relaxing in $ZnTiO_3$ structure. The XRD patterns of the $ZnTiO_3$ films observed that there were no diffraction peaks in the XRD pattern for as-deposited films due to the film structure is mainly amorphous. The hexagonal $ZnTiO_3$ phase was observed with the $ZnTiO_3$ (1 0 4), (1 1 0), (1 1 6), and (2 1 4) peaks at 620 °C. The intensities of the (1 0 4) peak was higher than the other peaks of $ZnTiO_3$ films at 820 °C, indicating that there is highly (1 0 4)-oriented $ZnTiO_3$ on the silicon substrate. The XPS core level analysis of the $ZnTiO_3$ films have been measured for O 1s, the change due to Zn–Ti complex compound that alter the H, M, R_{ms}, and R_a from annealing treatment. The average nanoindentation depth increased significantly upon increasing the annealing temperature, implying that higher annealing temperature resulted in weaker bonds, lower resistance, and decreased in strain energy at the film.

References

[1] F.H. Dulin, D.E. Rase, J. Am. Ceram. Soc. 43 (1960) 125.
[2] S.F. Bartram, R.A. Slepetys, J. Am. Ceram. Soc. 44 (10) (1961) 493.
[3] H.W. Yao, R.B. Feng, Min. Saf. Environ. Prot. 28 (2001) 20.
[4] S.F. Wang, M.K. L€u, F. Gu, C.F. Song, D. Xu, D.R. Yuan, G.J. Zhou, Y.X. Qi, Inorg. Chem. Commun. 6 (2003) 185.
[5] R.P. Gupta, S.K. Gangwal, S.C. Jain, U.S. Patent 5,714,431 (1998).
[6] H.T. Kim, Mater. Res. Bull. 33 (1998) 963.
[7] A. Golovchansky, H.T. Kim, Y.H. Kim, J. Korean Phys. Soc. 32 (1998) 1167.
[8] H.T. Kim, S. Nahm, J.D. Byun, J. Am. Ceram. Soc. 82 (1999) 3476.
[9] H. Obayashi, Y. Sakurai, T. Gejo, J. Solid State Chem. 17 (1976) 299.
[10] Z.X. Chen, A. Derking, W. Koot, M.P. van Dijk, J. Catal. 161 (1996) 730.
[11] K.H. Yoon, J. Cho, D.H. Kang, Mater. Res. Bull. 34 (1999) 1451.
[12] E. Hosono, S. Fujihara, M. Onuki, T. Kimura, J. Am. Ceram. Soc. 87 (2004) 1785.
[13] S.F. Wang, M.K. Lu, F. Gu, C.F. Song, D. Xu, D.R. Yuan, S.W. Liu, G.J. Zhou, Y.X. Qi, Inorg. Chem. Commun. 6 (2003) 185.
[14] S.F. Wang, F. Gu, M.K. Lu, C.F. Song, D. Xu, D.R. Yuan, S.W. Liu, Chem. Phys. Lett. 373 (2003) 223.
[15] H.T. Kim, Mater. Res. Bull. 33 (1998) 975.
[16] Y.S. Chang, Y.H. Chang, I.G. Chen, G.J. Chen, Y.L. Chai, J. Cryst. Growth 243 (2002) 319.
[17] Y.S. Chang, Y.H. Chang, J. Alloys Compd. 354 (2003) 303.
[18] Y.S. Chang, Y.H. Chang, Solid State Commun. 123 (2003) 203.
[19] Z.X. Chen, J. Eyden, W. Koot, R. Berg, J. Mechelen, A. Derking, J. Am. Ceram. Soc. 78 (1995) 2993.
[20] W.C. Oliver, G.M. Pharr, J. Mater. Res. 7 (1992) 1564.
[21] M.P. Pechini, US Patent No. 3231 (1996), p. 328.
[22] G.A. Hutchins, G.H. Maher, S.D. Ross, Am. Ceram. Soc. Bull. 66 (4) (1987) 681.
[23] P.F. Yang, H.C. Wen, Y.S. Lai, C.T. Wang, S. Wu, R.S. Chen, Microelectron. Reliab. 48 (2008) 389.
[24] D. Sreekantha Reddy, B. Kang, S.C. Yu, Y. Dwarakanadha Reddy, S.K. Sharma, K.R. Gunasekhar, K.N. Rao, P. Sreedhara Reddy, Curr. Appl. Phys. 9 (2009) 431.
[25] M.H. Lin, H.C. Wen, Y.R. Jeng, C.P. Chou, Nanoscale Res. Lett. 5 (11) (2010) 1812.
[27] Y.M. Chang, H.C. Wen, C.S. Yang, D. Lian, C.H. Tsai, J.S. Wang, W.F. Wu, C.P. Chou, Microelectron. Reliab. 50 (2011) 1111.
[28] J.S. Jung, Y.H. Kim, S.K. Gil, D.H. Kang, J. Electroceram. 23 (2009) 272.
[29] O. Yamaguchi, M. Morimi, H. Kawabata, K. Shimizu, J. Am. Ceram. Soc. 70 (1987) 97.
[30] B.R. Strohmeier, D.M. Hercules, J. Catal. 86 (1984) 266.
[31] A.R. Phani, M. Passacantando, S. Santucci, J. Phys. Chem. Solids 68 (2007) 317.
[34] Y.C. Lee, Y.L. Huang, W.H. Lee, F.S. Shieu, Thin Solid Films 518 (2010) 7366.